JOURNAL OF MATERIALS SCIENCE 32 (1997) 5225–5232

Interfacial structures and mechanical properties of steel–Ni and steel–Ti diffusion bonds

HIROSHI KATO, SHOJI ABE, TOSHIHIKO TOMIZAWA
Department of Mechanical Engineering, Faculty of Engineering, Saitama University, 255 Shimo-Okubo, Urawa, Saitama 338, Japan

Static and fatigue shear tests of steel–Ni bonds and steel–Ti bonds were carried out to obtain the relations between the strengths and the bonding conditions. Ultrasonic measurements were also made to examine the relations between the strengths and the size of the bonded region (the estimated diameter). At the bonding interface of the steel–Ni bonds, no intermediate phase was observed. At the bonding interface of the steel–Ti bonds, a thin layer of intermetallic compound was formed at lower bonding temperatures but, at higher bonding temperatures, the interlayer melted and the bonding interface became rough. The intensity of the ultrasonic wave reflected from the bonding interface changed, depending on the state of the bonding interface. In shear tests of the steel–Ni and steel–Ti bonds, cracks propagated along the bonding interface, and the strength was proportional to the square of the estimated diameter. In fatigue tests, cracks propagated in the thickness direction of the plate and no relation was obtained between the fatigue life and the estimated diameter. Fatigue life distributions were represented by two- and three-parameter Weibull distributions.

1. Introduction

Many machine parts are fabricated by the diffusion-bonding process. In bonding of dissimilar metals, however, some problems arise: appearance of residual stresses caused by mismatch of thermal expansions between bonding metals, and formation of brittle phases at a bonding interface. Recently, the shear strengths of diffusion bonds of dissimilar metals were measured [1], in which the strength of specimens with no intermediate phase at the bonding interface increased with increasing size of bonded region, but no relation was obtained between the strength and the size of the bonded region in specimens with intermediate phases. Since many machine parts suffer cyclic loading, it is important to clarify the fatigue properties of diffusion bonds. By the measurement of the strengths of diffusion bonds of steel plates [2, 3], the shear strength and fatigue life increased with increasing size of the bonded region. From these results, it is important to clarify the fatigue properties of diffusion bonds of dissimilar metals not only to contribute towards the design of machine parts but also to improve their reliability in use.

In the present work, steel plates were joined to nickel plates [4] and to titanium plates by diffusion bonding. In the former bonding, no intermediate phase is formed at the bonding interface and, in the latter bonding, an intermediate phase is formed. Diffusion bonds were subjected to shear and fatigue tests to obtain the relations between the strengths and the bonding conditions. Ultrasonic measurements were also carried out to obtain the relations between the strengths and the size of the bonded region estimated by the ultrasonic measurements. Results were compared with those of steel bonds [2, 3, 5].

2. Experimental procedures

2.1. Diffusion bonding

Plates of mild steel (C, 0.15–0.20 wt%; Mn, 0.3–0.6 wt%; P, $\leqslant$ 0.045 wt%; S, $\leqslant$ 0.045 wt%), nickel (99.0 wt% in purity) and titanium (99.9 wt% in purity) 5–5.5 mm in thickness were used in the present work. The mechanical properties of these metals are shown in Table I. In the table, heat-treated metals were heated at 1273 K for 30 s and then cooled to room temperature in air to simulate a thermal history in the bonding process. Rectangular plates 25 mm in width and 75 mm in length were sectioned from the plates and were polished by grinder. The surface roughness, R_{max}, of the plates was 2.7–3.5 μm after polishing.

The plates were rapidly bonded under a dynamic superplastic state. After cleaning by acetone, the plates were fixed between electrodes 20 mm in diameter as shown in Fig. 1 and then loaded with 16.2 MPa. The plates were heated to required temperatures (the maximum temperature) by sending an electric current through electrodes, and then the current was cut off to cool the plates to required temperatures (the minimum temperature equals the maximum temperature minus 300 K). The heating–cooling operation was repeated three times. The temperature in the bonding process was monitored with an alumel–chromel

0022–2461

TABLE I Mechanical properties of materials

Material		Yield strength (MPa)	Tensile strength (MPa)	Elongation (%)
Mild steel	As received	285	511	9
	Heat treated	232	380	21
Ni	As received	211	372	50
	Heat treated	50	345	54
Ti	As received	180	342	57
	Heat treated	107	390	26

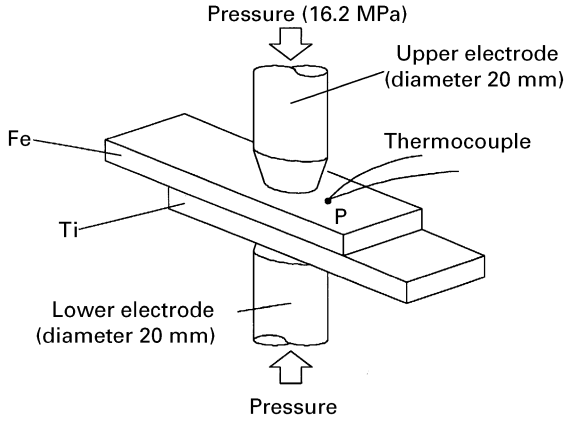

Figure 1 Set-up for diffusion bonding.

thermocouple of 0.3 mm diameter welded at a point about 1 mm from the end of the electrode on the surface of the steel plate.

2.2. Ultrasonic measurements

Ultrasonic measurements were carried out to estimate the size of the bonded region. After the surfaces of the bonded plates had been polished, a probe for generating and receiving a longitudinal wave of 5.0 MHz frequency was attached to the steel plate (the upper plate) at a contact pressure of 24.5 kPa, and the intensity of the first echo reflected from the bottom of the steel plate was measured along the plate axis at intervals of 1 mm. Machine oil was used as a couplant. From the echo intensity, an echo reflectivity, S, was obtained as follows:

$$S = 20 \log_{10}\left(\frac{B_x}{B_0}\right) \quad (1)$$

where B_x and B_0 are the echo intensities measured at the position x and at the end of the plate, respectively. Figure 2 shows a typical change in the echo reflectivity along the plate axis in the steel–Ni bonds.

The echo reflectivity (the theoretical echo reflectivity, S_{th}) was calculated under the following assumptions and compared with the measured echo reflectivity to estimate the size of bonded region.

1. The shape of the bonded region is a circle.
2. The ultrasonic wave propagates at a right angle to the surface of the plate without divergence.
3. The ultrasonic wave is reflected from the bonding interface with an interfacial reflectivity, α. When

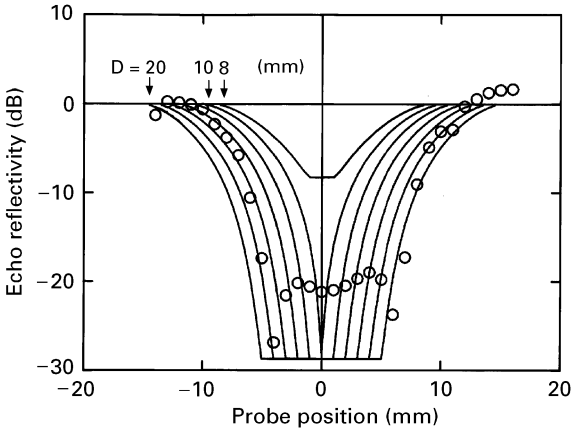

Figure 2 Typical changes of measured (○) and calculated (——) echo reflectivities along the plate axis of steel–Ni bonds.

the plates are not bonded, the ultrasonic wave is reflected from the bottom of the upper plate (the steel plate).

Typical changes in the theoretical echo reflectivity, S_{th}, are shown in Fig. 2. The theoretical reflectivity was compared with the measured reflectivity, and a diameter, D, giving the theoretical reflectivity in best agreement with the measured reflectivity was obtained by the least-squares approximation as an estimated diameter, D_u, of the bonded region.

2.3. Mechanical tests

After the ultrasonic measurements, static shear tests (hereafter referred to as the shear tests) and fatigue shear tests (hereafter referred to as the fatigue tests) of the bonded plates were carried out.

In the shear tests, the bonded plates were pulled in the axial direction of the plate at a cross-head speed of 8.3 μm s^{-1} (0.5 mm min^{-1}). In the tests, small plates of the same thickness as the bonded plates were inserted between the bonded plates and cramps to decrease the bending of the bonded plates during testing. The shear strength, τ ($= P_f/A$), was obtained with a load, P_f, at fracture and an area, A, of the face of the electrode attached to the plate. After the shear tests, the area of tear fracture (the area of the bonded region) was measured on the fracture surface, and the diameter of a circle with the same area as the bonded region was obtained as a measured diameter, D_B, of the bonded region.

Fatigue tests were carried out using the diffusion bonds bonded at 1273–1300 K under the following conditions: loading in the axial direction of the bonded plates, a sinusoidal change in load, a stress ratio of 0.1, and a frequency of 30 Hz. The S–N diagram was obtained from fatigue tests of different stress amplitudes using diffusion bonds of an estimated diameter of 18 mm or more. Fatigue limits were obtained as stress amplitudes to give a fatigue life of 1.0×10^7 or more. Then, fatigue life distributions were obtained by fatigue tests of stress amplitudes to give a fatigue life of $(1 - 5) \times 10^5$ using diffusion bonds of any estimated diameter.

3. Results and discussion

3.1. Structure at the bonding interface

Fig. 3 shows a typical microstructure at the bonding interface of the steel–Ni bonds. The bonding interface was planar and no intermediate phase was observed. By the electron probe microanalysis, iron and nickel changed smoothly with distance from the bonding interface. In the steel plate at the bonding interface, recrystallization occurred and the crystal grains coarsened. In the nickel plate at the interface, annealing twins appeared.

Macroscopic bonding interfaces in the steel–Ti bonds are shown in Fig. 4. When the plates were bonded at lower temperatures, a thin and planar layer (the maximum thickness, $\delta \approx 75\ \mu m$) appeared at the bonding interface, as shown in Fig. 5. When the plates were bonded at higher temperatures, the interlayer melted and became thick ($\delta \approx 800\ \mu m$), as shown in Fig. 6. Fig. 7 shows the distributions of iron and titanium in the interlayer of the diffusion bonds bonded at 1300 K. A quantitative analysis of the elements and the Fe–Ti binary phase diagram [6] showed that a eutectic structure of TiFe and β–Ti (melting temperature, 1358 K) was formed in the interlayer and melted in the bonding process. Although a chemical analysis was not carried out, the thin interlayer in the diffusion bonds bonded at lower temperatures was estimated to be the intermetallic compound TiFe from the phase diagram [6]. A Vickers hardness measurement with a load of 1.2 N gave the interlayer much higher values of 450–1150 HV than the values of iron and titanium of 170–200 HV, as shown in Fig. 8.

3.2. Relation between the estimated diameter and the bonding strength

The estimated diameter of the bonded region is shown as a function of the bonding temperature in Fig. 9. Although the estimated diameter of the steel–Ni bonds monotonically increased with increasing bonding temperature, the estimated diameter of the steel–Ti bonds changed in a complicated manner and the steel plate was not bonded to the titanium plate at 1050 K. In spite

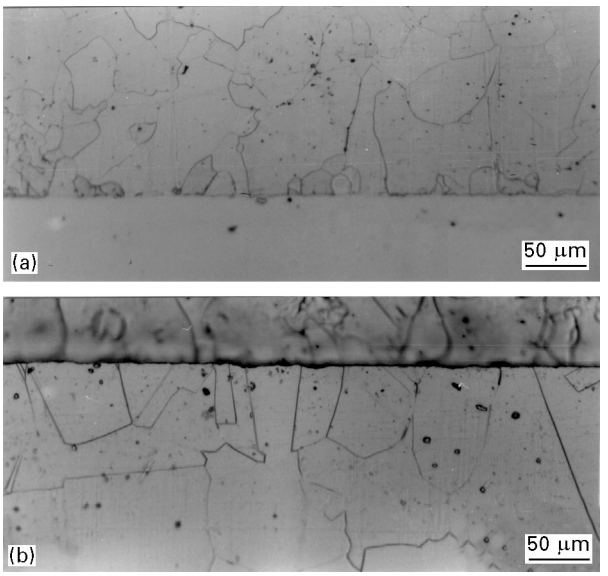

Figure 3 Microstructures at bonding interface of steel–Ni bonds: (a) etching of steel plate; (b) etching of nickel plate.

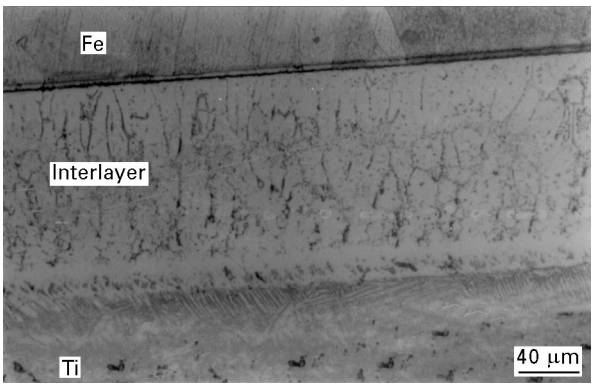

Figure 5 Microstructure at the bonding interface of steel–Ti bonds bonded at 900 K

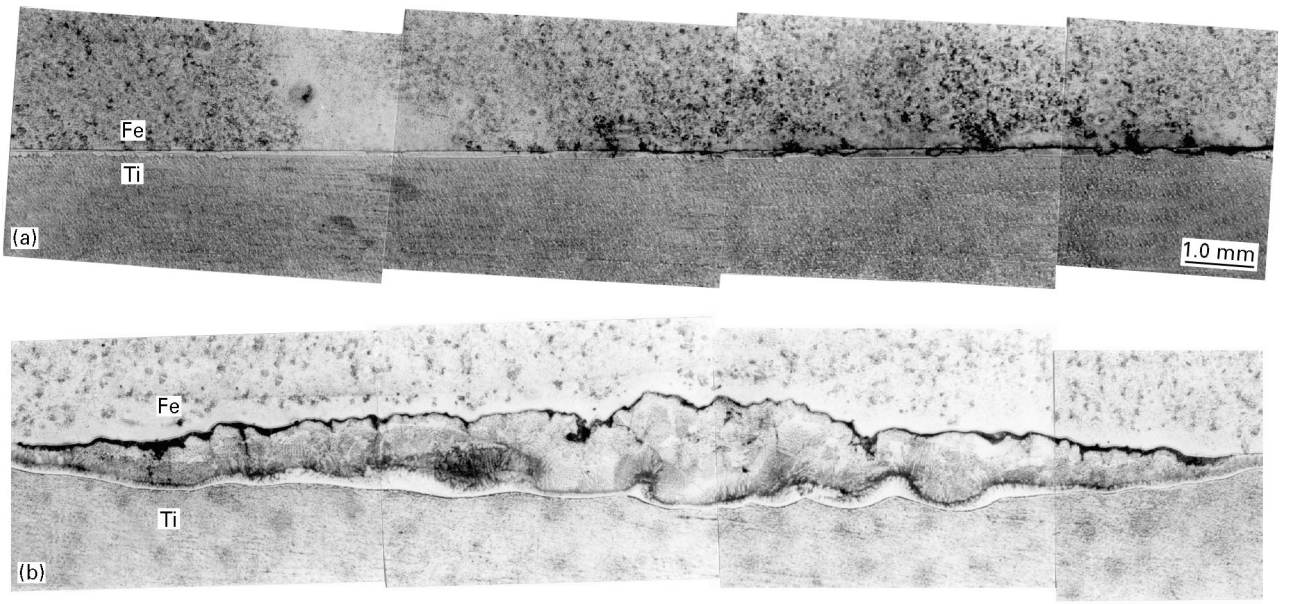

Figure 4 Macroscopic bonding interfaces of steel–Ti bonds: (a) specimen bonded at 900 K; (b) specimen bonded at 1300 K,

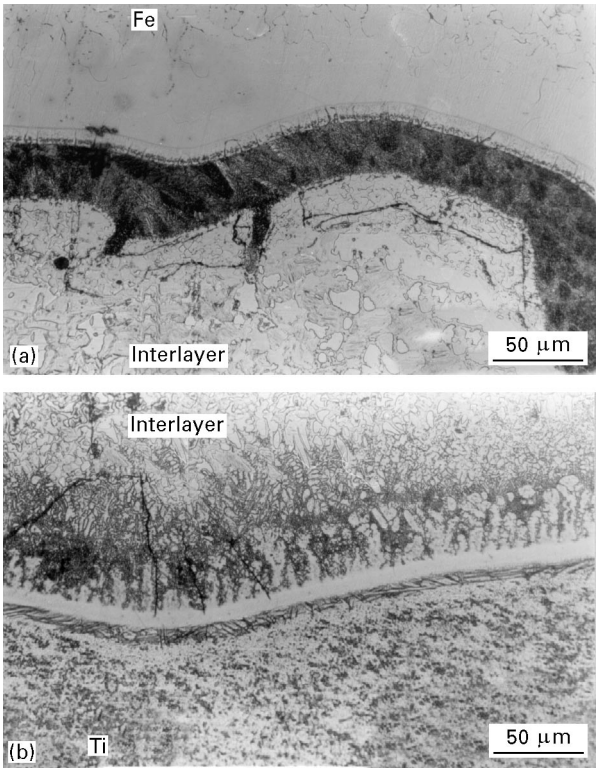

Figure 6 Microstructures at the bonding interface of steel–Ti bonds bonded at 1300 K: (a) boundary between steel and the interlayer; (b) boundary between titanium and the interlayer.

of various changes in the estimated diameter with the bonding temperature, the estimated diameter, D_u, had a linear relation with the diameter, D_B, of the bonded region such as $D_u = 1.4D_B$, as shown in Fig. 10.

No bonding of the steel–Ti bonds at 1050 K is caused by the excess of the thermal stresses over the bonding strength. When the bonding was done above the A_1 temperature of the steel, the steel plate was austenite, and then the steel plate transformed into ferrite during cooling after bonding, which caused large shear forces at the bonding interface. Moreover, a brittle layer was formed at the bonding interface. Therefore, after the plates were bonded at a temperature of 1000–1050 K, the bonded plates split away during cooling because of thermal stresses. At temperatures above 1100 K, superplastic deformation of metals, especially in titanium [7, 8], and melting of the interlayer occurred. These caused an increase in the area of the bonded region and a decrease in the residual stresses at the bonding interface, and the steel plate was joined to the titanium plate.

The change in the echo reflectivity along the plate axis was measured. In the case of the steel–Ni bonds, the echo reflectivity was almost constant in the bonded region, as shown in Fig. 2. In the case of the steel–Ti bonds, however, the echo reflectivity changed, depending on the state of the bonding interface. In the diffusion bonds bonded at lower temperatures, the echo reflectivity was almost constant in the bonded region, as shown in Fig. 11a. In the diffusion bonds bonded at higher temperatures, however, the echo reflectivity largely decreased below the theoretical value in the bonded region, as shown in Fig. 11b. When the bonding temperature was low and the plates

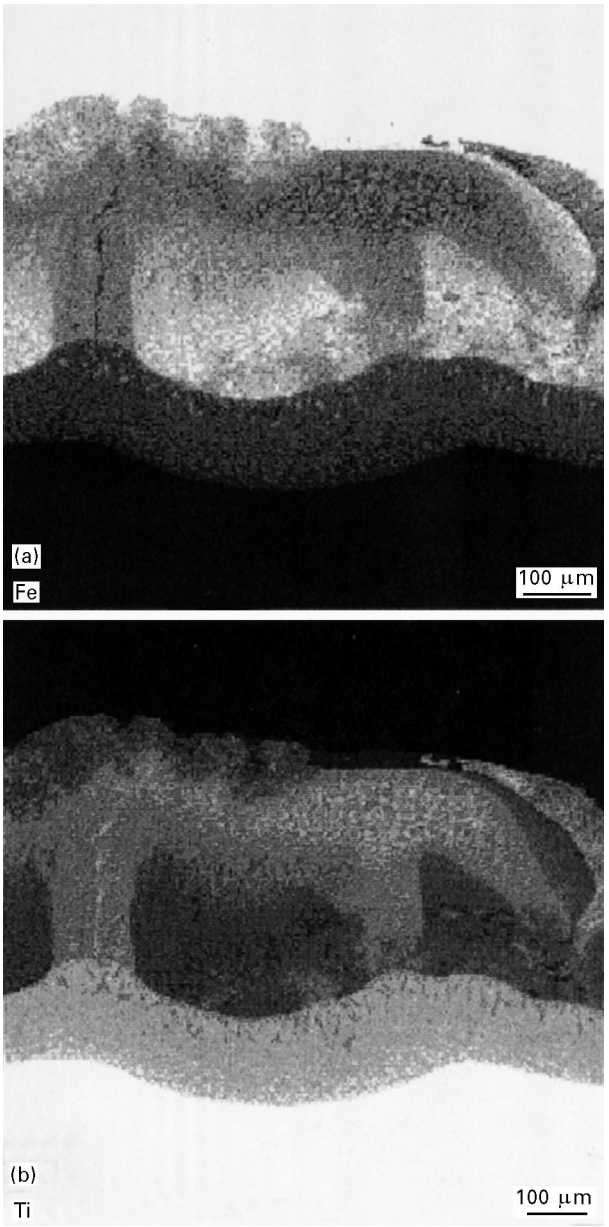

Figure 7 Distributions of iron and titanium in the interlayer of steel–Ti bonds bonded at 1300 K, where the brighter area contains a higher amount of the element: (a) iron; (b) titanium.

were bonded in a solid state, a thin planar interlayer was formed, as was observed in Fig. 4a, and the echo reflectivity was in good agreement with the theoretical value, as shown in Fig. 11a. However, when the bonding temperature was so high that the interlayer melted and the interface became rough, as was observed in Fig. 4b, the ultrasonic wave was largely scattered at the interface and the echo reflectivity decreased below the theoretical value, as shown in Fig. 11b. From these results, the state of the bonding interface in dissimilar metal bonds can be non-destructively evaluated by the ultrasonic measurement.

In the shear test, all diffusion bonds fractured along the bonding interface as in the case of the steel bonds. The temperature dependence of the shear strength was in good agreement with the temperature dependence of the estimated diameter, and a parabolic relation was obtained between the shear strength and the estimated diameter, as shown in Fig. 12. In the figure, the results of the steel bonds [3] are also presented. By

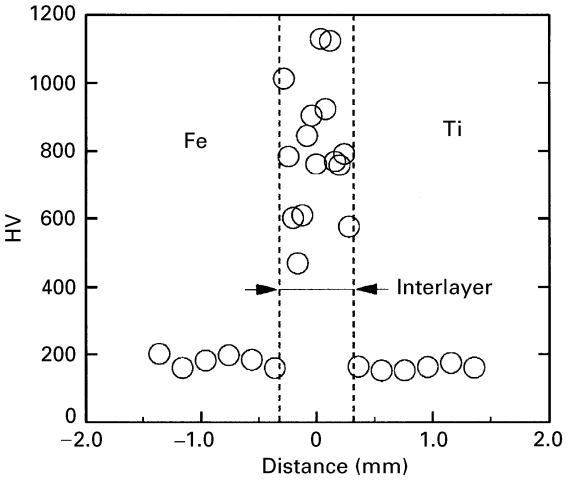

Figure 8 Vickers hardness at the bonding interface of steel–Ti bonds bonded at 1300 K.

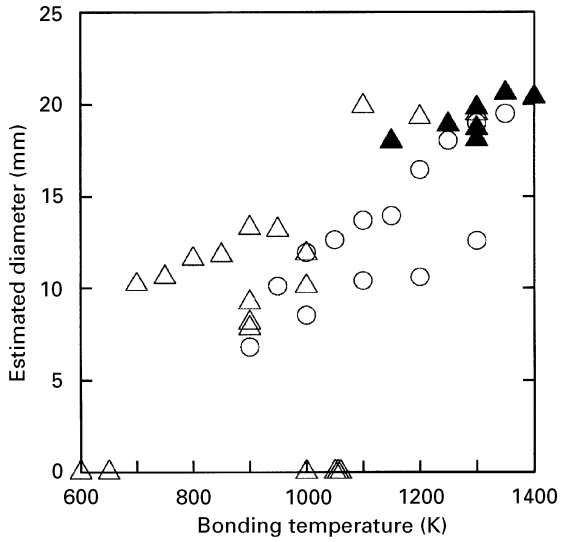

Figure 9 Variations in the estimated diameter of the bonded region with bonding temperature. (○), Steel–Ni bonds; (△), steel–Ti bonds when the echo intensity was almost constant in the bonded region as shown in Fig. 11a; (▲), steel–Ti bonds when the echo reflectivity is greatly decreased in the bonded region as shown in Fig. 11b.

using the least-squares approximation, the following relations are obtained between the shear strength, τ, and the estimated diameter, D_u:

$$\text{steel–Ni bonds: } \tau = 0.29\,D_u^2 \tag{2a}$$

$$\text{steel–Ti bonds: } \tau = 0.13\,D_u^2 \tag{2b}$$

$$\text{steel bonds [3]: } \tau = 0.15\,D_u^2 \tag{2c}$$

In [9, 10], stress intensity factors of the spot-welded joints under tensile shear were obtained, in which the stress intensity factors at the end of the bonded region are represented as follows:

$$K_I = \tau(\pi a)^{1/2}\,[0.605\,(a/b)^{0.397}] \tag{3a}$$

$$K_{II} = \tau(\pi a)^{1/2}\,[0.5 + 0.287\,(a/b)^{0.710}] \tag{3b}$$

where τ is the shear stress applied to the bonded region, a ($= D/2$) is the radius of the bonded region

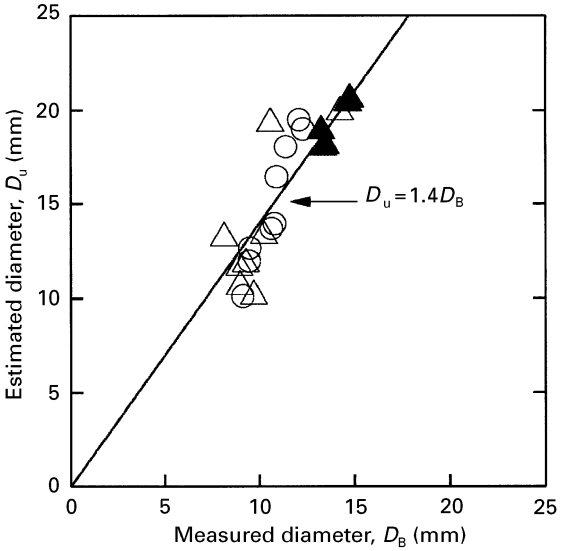

Figure 10 Relation between the estimated diameter, D_u, and the diameter, D_B, calculated from the measured area of the bonded region. The symbols are the same as in Fig. 9.

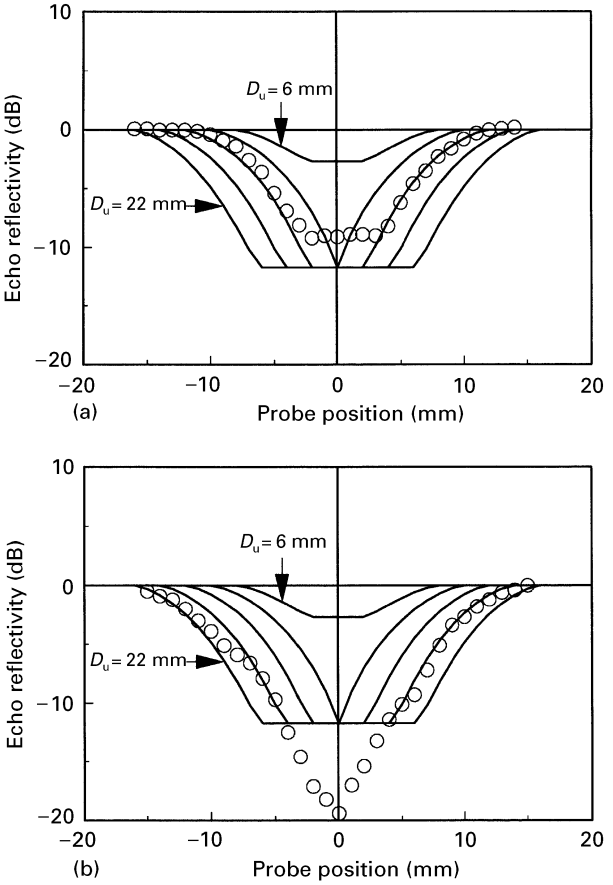

Figure 11 Typical changes in measured (○) and calculated (——) echo reflectivities along the plate axis of steel–Ti bonds: (a) specimen bonded at 900 K; (b) specimen bonded at 1300 K.

and b is half the plate thickness. Equations 3a and 3b are valid for bonds of the same materials. Since Young's moduli of steel (206 GPa) and Ni (200 GPa) are similar, these equations can be applied also to the case of the steel–Ni bonds. The ratio K_I/K_{II} is dependent only on a/b and, when the diameter,

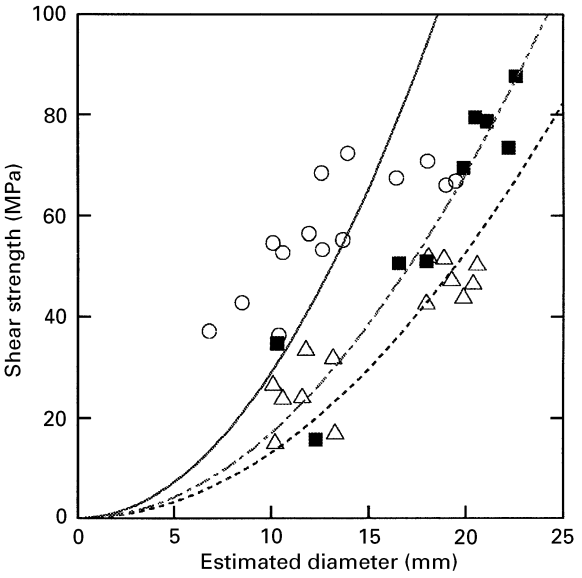

Figure 12 Relation between the shear strength and the estimated diameter. (○) (——), Steel–Ni bonds; (△) (- - - -), steel–Ti bonds; (■) (– – –), steel bonds.

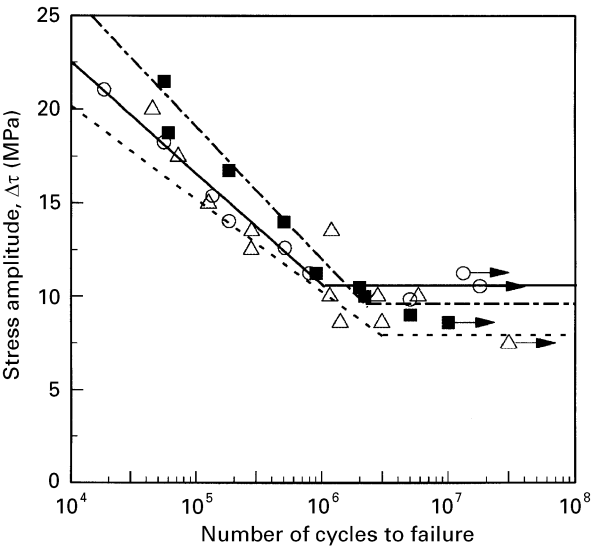

Figure 13 S–N diagram of diffusion bonds. The symbols are the same as in Fig. 12.

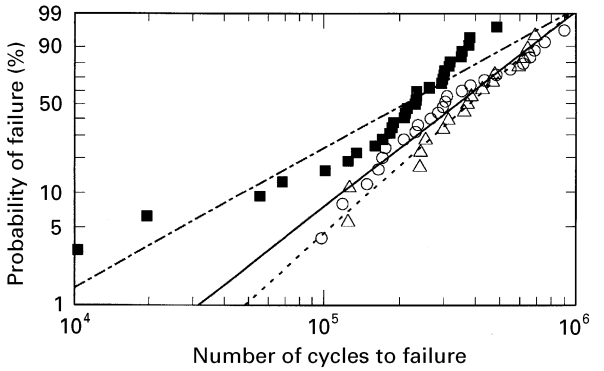

Figure 14 Relation between the cumulative probability of failure and the number of loading cycles to failure. The symbols are the same as in Fig. 12.

$D(=2a)$, of the bonded region changes from 5.0 to 25.0 mm, the ratio K_I/K_{II} changes from 0.821 to 0.991 at $2b = 5.0$ mm. Therefore, the stress intensity factor, K_{II}, of mode II is larger than the stress intensity factor, K_I of mode I, in the range of the present work ($D = 6.9$–19.5 mm). Since the critical stress intensity factors, K_{Ic} and K_{IIc} at the bonding interface are not known, however, it was not determined which mode was dominant in the fracture of the diffusion bonds.

Although no correlation was obtained between the shear strength and the estimated diameter for the steel–Ti bonds in the previous work [1], a good correlation was obtained between them in the present work. This difference was caused by the difference in the number of thermal cycles in the bonding process; the numbers of thermal cycle were 3 and 5 in the present work and in the previous work, respectively. On increasing the number of thermal cycles, the thickness of the interlayer increased and the bonding interface became brittle, decreasing the bonding strength, and there was no longer a correlation between the shear strength and the estimated diameter.

3.3. Relation between fatigue strength and estimated diameter

The *S–N* diagram was obtained for diffusion bonds with an estimated diameter of 18 mm or more, as shown in Fig. 13. At larger stress amplitudes, the stress amplitude linearly decreased with increasing logarithm of the number of cycles to fracture, and the following relations are obtained:

$$\text{steel–Ni bonds:} \quad \Delta\tau = 46.3 - 2.6 \log_{10} N \quad (4a)$$

$$\text{steel–Ti bonds:} \quad \Delta\tau = 40.0 - 2.2 \log_{10} N \quad (4b)$$

$$\text{steel bonds [3]:} \quad \Delta\tau = 54.4 - 3.1 \log_{10} N \quad (4c)$$

In the case of the steel–Ni bonds, cracks appeared at ends of the bonded region and propagated in the thickness direction of the plate (transverse fracture), which was the same as crack propagation in the steel bonds. In the case of the steel–Ti bonds, shear fracture along the bonding interface was expected because of the appearance of brittle phases at the bonding interface, but transverse fracture occurred at lower stress amplitudes. The shear fracture of the steel–Ti bonds occurred only at higher stress amplitudes. The fatigue limits were 10 MPa and 8 MPa for the steel–Ni and steel–Ti bonds, respectively. These values were in good agreement with the fatigue limit of the steel bonds, 10 MPa [3]. Since the crack propagated in the thickness direction of the plate in the fatigue tests, the resistance against the crack propagation was the same as the resistance of the base metal, and the fatigue limits of the steel–Ni and steel–Ti bonds agreed well with the fatigue limit of the steel bonds.

Fatigue life distributions were obtained by using diffusion bonds of any estimated diameters with stress amplitudes 12.6 MPa and 15.0 MPa for the steel–Ni bonds and the steel–Ti bonds, respectively, as shown in Fig. 14. Average fatigue lives of 3.4×10^5 and

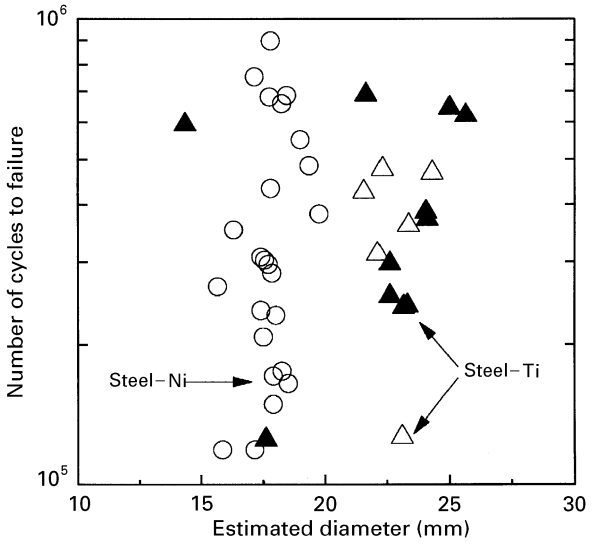

Figure 15 Relation between the number of loading cycles to failure and estimated diameter. (○), (△), transverse fracture; (▲), shear fracture.

3.8×10^5 were obtained for the steel–Ni bonds and the steel–Ti bonds, respectively. These values were in good agreement with the average fatigue life of the steel bonds, 2.1×10^5, obtained with a stress amplitude of 14.2 MPa. Fatigue life distributions were plotted on the two-parameter Weibull distribution curves with some scatter, and the following relations are obtained:

$$\text{steel–Ni bonds:} \quad F(N) = 1 - \exp\left[-\left(\frac{N}{4.16 \times 10^5}\right)^{1.79}\right] \tag{5a}$$

$$\text{steel–Ti bonds:} \quad F(N) = 1 - \exp\left[-\left(\frac{N}{4.49 \times 10^5}\right)^{2.06}\right] \tag{5b}$$

$$\text{steel bonds:} \quad F(N) = 1 - \exp\left[-\left(\frac{N}{2.77 \times 10^5}\right)^{1.23}\right] \tag{5c}$$

The fatigue life distributions of the steel–Ni bonds and the steel bonds curved downwards and upwards, respectively. No selection of specimens was done in the present fatigue test, and the steel–Ni bonds may have contained some groups of diffusion bonds with different average fatigue lives. The fatigue life distribution of the steel–Ni bonds was represented well by the three-parameter Weibull distribution as follows:

$$F(N) = 1 - \left[-\left(\frac{N - 0.77 \times 10^5}{3.24 \times 10^5}\right)^{1.21}\right] \tag{6}$$

Deviation of the steel bonds from the two-parameter Weibull distribution has been explained by various fracture modes: transverse fracture, shear fracture and twist fracture [2, 3].

The relation between the fatigue life and the estimated diameter was obtained with the same diffusion bonds used in Fig. 14, as shown in Fig. 15. In the case of the steel–Ni bonds, the fatigue life had a tendency to increase with increasing estimated diameter, but no relation was obtained in the steel–Ti bonds because of the large scatter of the data. The fatigue life may increase with increasing estimated diameter, but the effect of the estimated diameter was so small that a clear relation was not obtained between the fatigue life and the estimated diameter in the present work.

4. Conclusion

In the case of the steel–Ni bonds, the bonding interface was planar and no intermediate phase was formed. In the case of the steel–Ti bonds, a thin layer of intermetallic compound was formed at lower bonding temperatures and, at higher bonding temperatures, the layer of the eutectic phase melted and the bonding interface became rough. The change in the reflectivity of the ultrasonic wave along the plate axis depended on the state of the bonding interface.

In the shear tests of the steel–Ni bonds and the steel–Ti bonds, the cracks propagated along the bonding interface. The shear strength of the bonds increased with increasing square of the estimated diameter of the bonded region.

In the fatigue tests of the steel–Ni bonds and the steel–Ti bonds, cracks appeared at the ends of the bonded region and propagated in the thickness direction of the plate. In the case of the steel–Ti bonds, fracture along the bonding interface occurred at higher stress amplitudes. Fatigue lives of the diffusion bonds were insensitive to the estimated diameter of the bonded region. Fatigue life distributions were represented by the two- and three-parameter Weibull distributions.

Acknowledgements

The authors would like to thank Mr T. Yamada and Mr K. Saito for their help in the experiment. The present work was performed under the financial support of the Japanese Ministry of Education, Science, Culture and Sports.

References

1. M. HONDA, H. KATO and K. YOSHIKAWA, *J. Soc. Mater. Sci., Jpn* **37** (1988) 837.
2. H. KATO, K. KANNO and K. YOSHIKAWA, in "Proceedings of the Sixth International Conference on the Mechanical Behaviour of Materials", Vol. 4, Kyoto, July 1991, edited by M. Jono and T. Inoue (Society of Materials Science, Japan, 1991) p. 741.
3. K. YOSHIKAWA, Research Report "Non-Destructive Evaluation of Fatigue Properties of Diffusion Bonds" (Grant-in-Aid for Scientific Research (B) of Japanese Ministry of Education, Science, Culture and Sports, Grant 1460224) (1991).
4. H. KATO, T. TOMIZAWA and K. YOSHIKAWA, in "Proceedings of the Conference on Advance Technology in Experimental Mechanics", Kanawaga, July 1993 (Japanese Society of Mechanical Engineers, Tokyo, 1993) p. 101.

5. M. SHIBATA, H. KATO, M. HONDA and K. YOSHIKAWA, *J. Jpn. Soc. Non-Destruct. Inspection* **35** (1986) 787.
6. T.B. MASSALSKI (ed.-in-chief), "Binary alloy phase diagrams", Vol. 1, (American Society for Metals, Metals Park, OH, 1986) p. 1084 (Fe–Ni system) and p. 1118 (Fe–Ti system).
7. M. MIYAGAWA (ed.-in-chief), "Superplasticity and metal-working technology", (Nikkan-Kogyo-Shinbun, Tokyo, 1980) pp. 75 and 82.
8. H. KATO, M. SHIBATA and K. YOSHIKAWA, *Mater. Sci. Technol.* **2** (1986) 405.
9. Y. MURAKAMI (ed.-in-chief), "Stress intensity factors handbook", Vol. 2 (Pergamon, Oxford, 1987) p. 1201.
10. L. P. POOK, *Int. J. Fract.* **11** (1975) 173.

Received 8 December 1995
and accepted 10 March 1997